

Real-time simulation of large-scale HTS systems: multi-scale and homogeneous models using T - A formulation

Edgar Berrospe-Juarez¹, Víctor M R Zermeño², Frederic Trillaud³ and Francesco Grilli⁴

¹Postgraduate School of Engineering, National Autonomous University of Mexico, Mexico

²NKT

³Institute of Engineering, National Autonomous University of Mexico, Mexico

²Karlsruhe Institute of Technology, Germany

email: eberrospej@iingen.unam.mx

This work was supported in part by the Programa de Maestría y Doctorado en Ingeniería of the Universidad Nacional Autónoma de México (UNAM) and the Consejo Nacional de Ciencia y Tecnología (CONACYT) under CVU: 490544, and by DGAPA-UNAM grant, PAPIIT-2017 #TA100617.

Abstract: The emergence of second-generation high temperature superconducting tapes has favored the development of large-scale superconductor systems. The mathematical models capable of estimating electromagnetic quantities in superconductors have evolved from simple analytical models to complex numerical models. The available analytical models are limited to the analysis of single wires or infinite arrays that, in general, do not represent real devices in real applications. The numerical models based on finite element method using the H formulation of the Maxwell's equations are useful for the analysis of medium-size systems, but their application in large-scale systems is problematic due to the excessive computational cost in terms of memory and computation time. Then it is necessary to devise new strategies to make the computation more efficient. The homogenization and the multi-scale methods have successfully simplified the description of the systems allowing the study of large-scale systems. Also, efficient calculations have been achieved using the T - A formulation. In this manuscript, we derived the adequate order of the elements used in the T - A formulation to avoid spurious oscillations in the current density. More importantly, we propose a series of adaptations to the multi-scale and homogenization methods so that they can be efficiently used in conjunction with the T - A formulation. The computation time and the amount of memory are substantially reduced up to a point that it is possible to achieve real-time simulations of slow ramping cycles of practical importance on laptop computers.

Keywords: Simulation of superconductors, current density distribution, hysteresis losses, large-scale HTS systems, magnetic field distribution, T - A formulation.

1. Introduction

In recent years important progress has been achieved in the manufacturing of high current, high temperature superconductors (HTS). Nowadays, the high current capacity of second-generation (2G) HTS tapes has made possible the production and the commercialization of superconducting fault current limiters and cables. The interest in the technology has spawned over to other large-scale superconducting systems such as generators, motors [1], and high field scientific magnets [2-4]. These devices are considered as large-scale systems, because they are made from hundreds to thousands of turns of HTS tapes. The design and operation of those systems are challenged by the difficulty of extracting the heat produced by the hysteresis losses. For particular applications such as the generation of high magnetic field, in addition to the estimation of the losses, it is required to compute accurately the local magnetic field and current density.

The first available analytical models were limited to the analysis of one single conductor [5-7]. More complex models considering conductor stacks under particular conditions are presented in [8-11]. The reader can refer to [12] for a thorough review of existing analytical models. On the other hand, numerical models opened up the possibility of considering systems with larger number of tapes. Methods like the finite element method (FEM) are well documented in the literature [13-15] and have been extensively applied to superconductor systems. Nevertheless, they have specific characteristics that should be considered in order to successfully address the modelling task [15-17]. For a deeper review of numerical models, the reader is referred to [18-19]. Among the available methodologies suitable for the analysis of large-scale systems, one should also mention the Minimum Magnetic Energy Variation (MMEV) method introduced in [20-21]. The MMEV method has evolved into the Minimum Electro-Magnetic Entropy Production (MEMEP) method [22-23].

The FEM models of HTS tapes use different formulations of Maxwell's equations. The differences between the formulations come from the variety in the choice of the state variables. The first proposed FEM model of an HTS tape used the $T-\phi$ formulation [24], a later model applied the $A-V$ formulation [25]. Other formulations are listed in [17] and [26]. During the last years the H formulation [26] has been widely used in the community. In two recent publications [27-28], the $T-A$ formulation has been proposed as an efficient approach to simulate thin superconductors. This formulation couples the T and A formulations, the computations are efficient enough to address the analysis of large-scale HTS systems. However, investigating the $T-A$ formulation further, we found that non-physical spurious oscillations may appear on the distribution of current density. Similar issues have already been reported in fluid mechanics literature [29-30], where different order elements are used to approximate velocity and pressure. As a prelude to the applications of the new proposed $T-A$ multi-scale and $T-A$ homogeneous strategies, we address the analysis of the order of the elements used in the $T-A$ formulation to find a stable pair of finite element spaces. The analysis is conducted by means of performing different simulations using different order of elements to approximate \mathbf{T} and \mathbf{A} .

The main concern when dealing with large-scale HTS systems is the large number of turns. The homogenization and the multi-scale approaches can considerably reduce the computational cost of the models without compromising accuracy. The homogenization process assumes that a stack of tapes can be represented by a single homogeneous anisotropic bulk. This approach was first proposed in [31] and later improved in [32-34]. The multi-scale approach is based on the idea of simulating a

subset of tapes, referred to as analyzed tapes. The interaction between a single tape and the full model made of all the tapes is achieved by computing the magnetic field generated by all the tapes. The magnetic field at the boundary of the analyzed tapes is then used as boundary condition to solve the current density in the analyzed tapes. This method was proposed in [35], with later refinements added in [36]. The last version of the method incorporates an iterative process to improve the accuracy of the current density in the analyzed tapes and, consequently, of the losses [37].

In this manuscript, two strategies, multi-scale and homogenization, used together with the T - A formulation are presented to address the numerical modelling of large-scale HTS systems. To couple those strategies with the proposed T - A formulation, some specific derivations are required. It is demonstrated that the proposed strategies can achieve real-time simulations of real charge/discharge cycles using a laptop computer.

This manuscript is organized as follows: Section 2 makes a brief presentation of the T - A formulation [27-28]. Section 3 contains the description of the case study, a racetrack coil made of 2000 turns. This case study and its H formulation model are used to validate the T - A formulation model as well as the choice of the order of the elements. The description of new proposed T - A multi-scale and homogeneous models is presented in section 4. Section 5 contains the validation of the multi-scale and homogenous models by comparing them with the previously validated T - A full mode, the results demonstrate the real-time capabilities of the proposed models. The conclusions are exposed in section 6. An appendix is also included to show the computation time limitations of the H formulation models.

2. T - A formulation

Hereinafter, we briefly recall some of the salient information of T - A formulation. For further information, the reader is referred to as [27-28].

Assuming the bounded universe is made of superconductive and non-conductive media, the T - A formulation relies on the current vector potential \mathbf{T} defined exclusively over the superconductive medium and the magnetic vector potential \mathbf{A} defined over the entire bounded universe. The corresponding boundary conditions are applied to the vector \mathbf{A} at the boundary of the universe. The current is assumed to circulate only in the superconducting layers and the rest of the universe is considered non-conductive.

The governing equation of the A formulation is

$$\nabla \times \nabla \times \mathbf{A} = \mu \mathbf{J}, \quad (1)$$

where μ is the magnetic permeability, \mathbf{J} the current density, and \mathbf{A} the magnetic vector potential defined as $\mathbf{B} = \nabla \times \mathbf{A}$, where \mathbf{B} is the magnetic flux density [26].

The governing equation of the T formulation is

$$\nabla \times \rho \nabla \times \mathbf{T} = -\frac{\partial \mathbf{B}}{\partial t}, \quad (2)$$

where ρ is the resistivity and the current vector potential is given by $\mathbf{J} = \nabla \times \mathbf{T}$ [26].

In the 2D case depicted in figure 1, the thickness of the superconducting layers is neglected, and the HTS tapes can be represented by 1D lines. Therefore, \mathbf{T} has a single scalar component T_y , and equation (2) is reduced to

$$\frac{\partial}{\partial x} \left(\rho_{HTS} \frac{\partial T_y}{\partial x} \right) = \frac{\partial B_y}{\partial t}, \quad (3)$$

where ρ_{HTS} is the resistivity of the HTS material. The magnetic field component B_y is obtained by calculating \mathbf{A} with the A formulation. The current density has only one component defined by $J_z = \partial T_y / \partial x$. Also, \mathbf{A} has only one component, A_z . The necessary boundary conditions at the edges of the superconducting layer for \mathbf{T} can be obtained by considering the transport current in the tape and the flux of the current density over the cross-section of the tape, as follows:

$$I = \iint_S \mathbf{J} dS = \iint_S \nabla \times \mathbf{T} dS = \oint_{\partial S} \mathbf{T} dr, \quad (4)$$

where S is the cross-section, and ∂S is its boundary. As shown in figure 1, the component of \mathbf{T} parallel to the tape is zero, then (4) is reduced to

$$I = (T_1 - T_2)\delta \quad (5)$$

where δ is the real thickness of the HTS layer. T_1 and T_2 are the potentials at the extremities of the tape as shown in figure 1. Thus, a different transport current can be impressed by modifying T_1 and T_2 on the edges of the HTS layer.

The current density is multiplied by the thickness of the HTS layer (δ), to obtain a surface current density $\mathbf{K} = J_z \cdot \delta$. The surface current density \mathbf{K} is impressed into the A formulation as an external surface current density by means of a boundary condition of the form

$$n \times (\mathbf{H}_1 - \mathbf{H}_2) = \mathbf{K} \quad (6)$$

where n the unit vector normal to the tape, while \mathbf{H}_1 and \mathbf{H}_2 are the magnetic field strength vectors above and below of the tape, respectively.

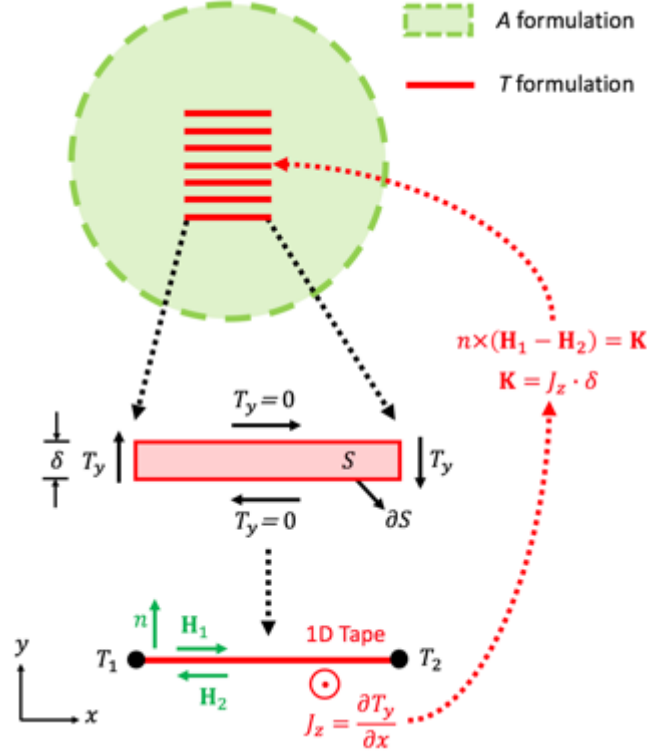


Figure 1. Bounded universe with superconductive layers and non-conductive media. The current vector potential \mathbf{T} is computed over the HTS layers and the magnetic vector potential \mathbf{A} is computed over the entire bounded universe. The surface current \mathbf{K} is impressed in by means of a boundary condition. The rectangle S is used in this figure just show how the boundary conditions are deduced, actually for the propose of computing both \mathbf{T} and \mathbf{A} , the superconductor layer is considered as a 1D line.

3. Case study and full models

H full model

The case study used in this manuscript is the same racetrack coil used in [36]. The coil has 10 pancakes (stacks), each composed of 200 turns. The symmetry allows to model just one quarter of the system, this means it is possible to consider 5 pancakes each one with 100 tapes.

The reference model of this section is also the same reference model used in [36]. This model uses the *H* formulation considering each tape, and is called *H full model*. We refer to the regions containing just one HTS layer and its surrounding medium as unit cells. The mesh of the unit cells is structured, and considers 1 element along the tape's thickness and 100 elements along its width. The 100 elements are distributed symmetrically with respect to the center of the tape with an increasing number of elements at the extremities of the tape. The copper and other normal conductors being part of the HTS tapes, as well as the cryogenic liquid have typical resistivity values several orders of magnitude bigger than those of superconductor material. Thus, the presence of the normal conductors

is neglected and the HTS layers are considered to be surrounded with a medium having a resistivity value $\rho_a = 1 \text{ } \Omega\text{m}$, see figure 1.

The electrical resistivity of the HTS material is modeled by the so-called E - J power-law [38],

$$\rho_{HTS} = \frac{E_c}{J_c(\mathbf{B})} \left| \frac{\mathbf{J}}{J_c(\mathbf{B})} \right|^{N-1}. \quad (7)$$

The critical current density J_c is defined by a modified Kim's relation [39], this relation describes the anisotropic dependence of the on the magnetic field

$$J_c(\mathbf{B}) = \frac{J_{c0}}{\left(1 + \sqrt{\frac{k^2 B_{\parallel}^2 + B_{\perp}^2}{B_0}} \right)^{\alpha}}, \quad (8)$$

where B_{\perp} and B_{\parallel} are the magnetic field components perpendicular and parallel to the wide surface of the tape. Since there are no magnetic materials, the permeability of the air and the HTS material is chosen to be the permeability of the vacuum μ_0 . The parameters of racetrack coil are summarized in table 1.

Table 1. Case study coil parameters.

Parameter	Value
Pancakes	10
Turns per pancake	200
Unit cell width	4.45 mm
Unit cell thickness	293 μm
HTS layer width	4 mm
HTS layer thickness	1 μm
E_c	1e-4 Vm^{-1}
N	38
J_{c0}	2.8e10 Am^{-2}
B_0	0.04265 T
k	0.29515
α	0.7
Surrounding medium ρ_a	1 Ωm

***T*-*A* full model**

The *T*-*A* full model of the case study is a model that uses the *T*-*A* formulation and considers all the tapes, this means that \mathbf{T} is computed in every tape. The mesh used in the unit cells domains is a

structured mesh, with 60 elements along the tape's width. The geometry and the mesh of the model is shown in figure 2. This figure also shows the numbering of the tapes and pancakes.

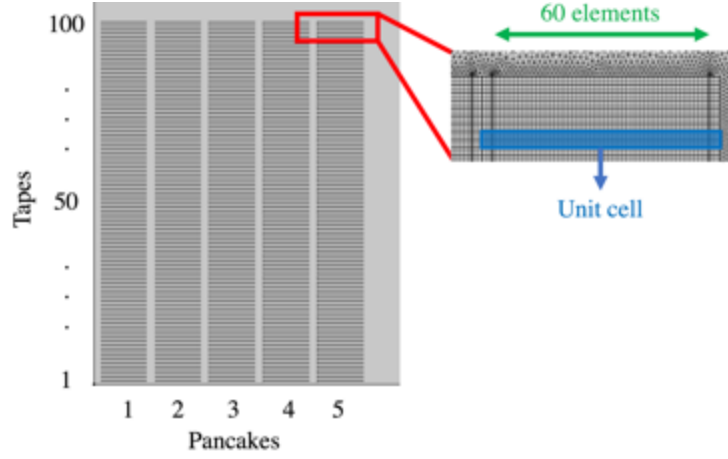


Figure 2. Geometry and mesh of the T - A full model. The analyzed section of the case study has 5 pancakes with 100 tapes per pancake. The mesh in the unit cells is structured.

Spurious oscillations in \mathbf{J}

To validate the T - A full model, the H full model and the T - A full model were simulated for one cycle of a 11 A, 50 Hz transport current. The value 11 A was chosen because at this current value the tape 1 in pancake 5 is completely penetrated by transport or magnetization currents. As discussed in the previous section, the T - A formulation uses two state variables, \mathbf{T} and \mathbf{A} . Each variable can be approximated using elements of different order. To assess the correct choice of orders, the T - A full model was simulated three times. The first simulation uses first order elements for both \mathbf{T} and \mathbf{A} , the second simulation uses second order elements for both variables, while the last simulation uses first order elements for \mathbf{T} and second order elements for \mathbf{A} .

The J distributions at the peak of transport current ($t = 15$ ms) computed with both H and T - A full models are shown in figure 3. The normalized current density ($J_n = J/J_c$) throughout the full system is presented in the first row, while the J in tape 96 of pancake 3 is presented in the second row. The results show that the J distributions of the T - A models present spurious oscillations when the same order of elements is used to approximate both \mathbf{T} and \mathbf{A} variables. It is possible to observe that the spurious oscillations are present at subcritical current densities values. Also, the period of the oscillations when first order elements are used for both variables is twice the period when second order elements are used for both variables. The oscillations disappear when first order elements are used for \mathbf{T} and second order for \mathbf{A} , then we assume this the correct choice of orders. These oscillations have not been discussed in previous literature about the T - A formulation.

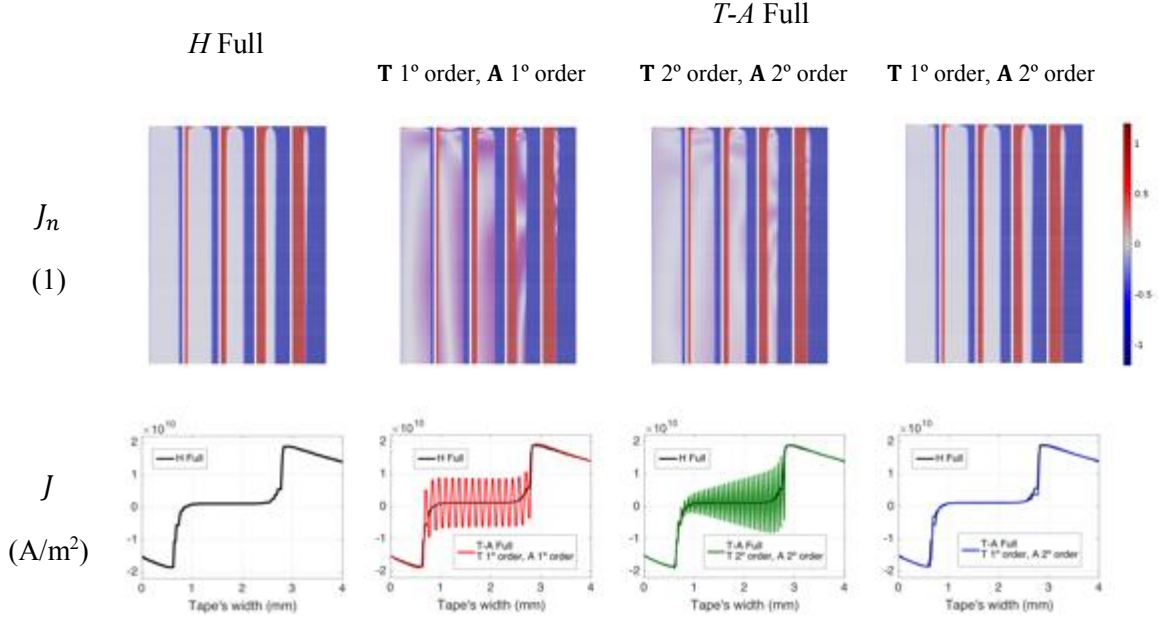


Figure 3. H full and T - A full models J distribution at peak transport current $t = 15$ ms. The first row shows J_n in the full system. The second row shows J in the tape 96 of pancake 3. The simulations were performed with the H formulation reference model and with the T - A full model. The T - A full model uses different order elements for \mathbf{T} and \mathbf{A} . The spurious oscillations are present when the same order is used for both variables.

The quantitative comparison of the H and T - A full models is carried out by calculating the relative error of the average hysteresis losses and the coefficient of determination (R^2) of the J distributions. The average hysteresis losses can be obtained considering data of the second half of the cycle, as follows,

$$Q_{av} = \frac{2}{P} \int_{P/2}^P \int_{\Omega} \mathbf{E} \cdot \mathbf{J} d\Omega dt, \quad (9)$$

where P is the period of the sinusoidal cycle, and Ω is the superconductor domain. The relative error on the losses is defined as $er_q = |(Q_{H_{av}} - Q_{TA_{av}})/Q_{H_{av}}| \times 100 \%$, where $Q_{H_{av}}$ and $Q_{TA_{av}}$ are the losses computed with the H and T - A full models respectively. The coefficient of determination is a widely used metric to evaluate the goodness of a fit [40], here we use it to compare the J distributions. The coefficient of determination is defined as,

$$R^2 = 1 - \frac{\sum_{i=1}^m (J_H - J_{TA})^2}{\sum_{i=1}^m (J_H - \bar{J}_H)^2}, \quad (10)$$

where J_H and J_{TA} are vectors containing the uniformly sampled J distributions over the tape width of all the tapes, for all the time steps, computed with the H and $T-A$ models, respectively.

Table 2. H and $T-A$ full models comparison.

Model		Av. Losses (W/m)	Relative error (%)	R^2 of J	Computation time
	H full	127.2389			31h 32min
$T-A$ full	T 1°, A 1° order	126.0212	0.96	0.8905	02h 46min
	T 2°, A 2° order	126.3897	0.67	0.9884	09h 01min
	T 1°, A 2° order	128.0560	0.64	0.9922	03h 14 min

The average losses, the losses relative error, the R^2 , and the computation time are summarized in table 2. As previously mentioned spurious oscillations are present at subcritical values, then they do not have an important impact in the hysteresis losses. The estimated losses of the $T-A$ models agree with the H full model with less than 1 %, but the lower error is achieved with the model using first order elements for **T** and second order elements for **A**. The impact of the oscillations is clearly reflected in the R^2 values. The R^2 value of the model using second order elements for both variables is larger than the R^2 of the model using first order elements for both variables, because the amplitude of the oscillations is lower, as can be seen in figure 3. The model with the larger R^2 value is the model using first order elements for **T** and second order elements for **A**, the one without spurious oscillations. Throughout the rest of this manuscript it is assumed that the $T-A$ models are models using first order elements for **T** and second order elements for **A**, unless otherwise indicated.

Another important aspect to consider is the computation time, all the models discussed in this manuscript were implemented in COMSOL Multiphysics 5.3, and the computer used to perform the simulations was a MacBook (3 GHz Intel Core i7-4578U, 4 cores, 16 GB of RAM). The three $T-A$ full models have a computation time significantly lower than the H full model. The increment in the order of the elements leads to the increment in the degrees of freedom (DOF), and the computation time, then the computation time when second order elements are used for both variables is almost three times the time of the model with first and second order elements. It should be mention that with the software used in this manuscript it was not possible to run simulations using second order elements for **T** and first order elements for **A**.

Numbers of elements along the tape's width

To assess the impact of the numbers of elements along the tape's width, the $T-A$ full model was modified to consider different number of elements ranging from 25 to 150. The distribution of the elements along the tape's width is uniform. It should be recalled that in the H full reference model an increasing number of elements is considered at the extremities of the tapes. That is why this assessment goes beyond the 100 elements considered in the H full model.

The results of the simulations using different number of elements are resumed in figure 4. The losses relative error and R^2 are plotted as a function of the number of elements along the tape's width. The less elements the larger losses error and the lower the R^2 . As the number of elements is incremented the relative error and R^2 present an asymptotic behavior. An extra axis is included in the upper part of the plot to report the computation time, it can be observed that the increment in the number of elements produces an increment in the computation time, and when the number of elements is 150 the computation time is more than the time required by the H full model. We consider that the compromise between accuracy and computation time is fulfilled with 60 elements along the tape's width, because with this number of elements the losses error is lower than 1 % and the R^2 is larger than 0.99. Throughout the rest of this manuscript it is assumed that the $T-A$ model has 60 elements along the tape's width.

To finish this section, figure 5 shows the average hysteresis losses in the coil, following the numbering presented in figure 2. The x-axis in the plots represents the tape's number, there are five lines, each one representing a different pancake. The losses in pancake 5 are almost three orders of magnitude larger than the losses in pancake 1. This difference is linked to the higher current penetration in the tapes across the pancakes, and to the difference in the field direction. The plots in figure 5 demonstrate that the $T-A$ full model can achieve accurate estimations of the electromagnetic quantities at a local level, this means along each individual tape.

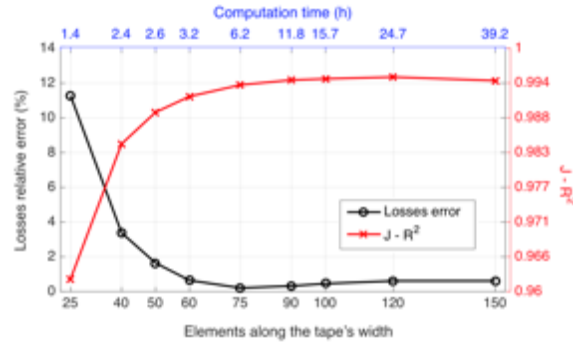


Figure 4. Losses relative error and coefficient of determination (R^2) of the J distribution as a function of the number of elements along the tape's width. The accuracy improves as the number of elements increase, but both parameters show and asymptotic behavior. The upper axis shows the computation time.

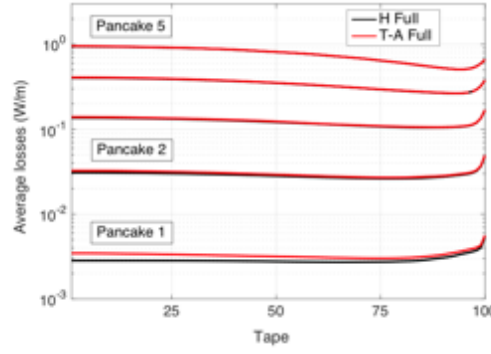


Figure 5. Average losses as a function of the tape's number inside each pancake, computed with the H and $T-A$ full models. The $T-A$ model use first order elements for \mathbf{T} and second order elements for \mathbf{A} , as well as 60 elements along the tape's width.

4. $T-A$ multi-scale and homogeneous approaches

This section presents two refined strategies, based on the $T-A$ formulation, that make use of less resources to obtain similar accuracies for the hysteresis losses as well as current density and magnetic field distributions.

$T-A$ multi-scale approach

The multi-scale method, as presented in [36-37], uses two different submodels. The single tape submodel use the H formulation and computes the J distribution in the analyzed tapes, while the coil submodel use the A formulation and computes the magnetic field throughout the full system. The multi-scale approach proposed here is based on the $T-A$ formulation, and there is only one model in which the T and A formulations are coupled together. Hence, these new multi-scale models are able to compute simultaneously the J distribution in the analyzed tapes and the background field produced by all the tapes.

The multi-scale $T-A$ models consider a reduced number of analyzed tapes whereby \mathbf{T} is exclusively defined. The J distributions along each analyzed tape is obtained by calculating \mathbf{T} with the T formulation. The J distributions in the non-analyzed tapes are approximated by linear interpolation of J in the analyzed tapes. The potential \mathbf{A} is defined over the entire bounded universe and its computation in turn allows the computation of \mathbf{B} . The J in the analyzed and non-analyzed tapes is multiplied by the thickness of the HTS layer (δ), to obtain a surface current density (\mathbf{K}) which is impressed into the A formulation by means of a boundary condition of the form (6). Figure 6 shows the multi-scale approach applied to a small stack.

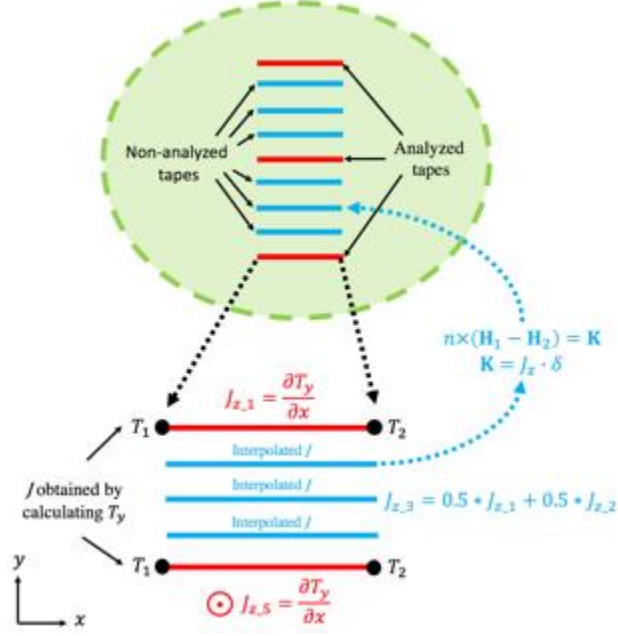


Figure 6. *T-A* multi-scale approach. In this example, there are 3 analyzed tapes whereby J is obtained by computing \mathbf{T} . The J in the rest non-analyzed tapes is approximated by linear interpolation. The surface current \mathbf{K} is impressed in by means of boundary conditions.

***T-A* homogenous approach**

The homogenization technique assumes that a stack of HTS tapes can be modeled as a homogeneous anisotropic bulk [34]. This simplification in the geometrical description should not compromise the electromagnetic behavior. The transformation of a small stack into a bulk that brings together all the unit cells containing the HTS tapes is depicted in figure 7.

Once again, \mathbf{A} is defined all over the entire bounded universe, while \mathbf{T} is now only defined inside the bulk. Inside the bulk, for the propose of computing \mathbf{T} , the influence of the component of \mathbf{B} parallel to the surface of the tapes is not considered, therefore \mathbf{T} is forced to have only one component. In the example show in figure 7, T_y is the only one component of \mathbf{T} and is defined by means of equation (3).

The bulk can be understood as the limiting case of a densely packed stack made up of tapes having an infinitesimal thickness. Each infinitesimal tape should transport the same current of its original counterpart, which in turn requires the boundary conditions T_1 and T_2 , defined in equation (5), to be applied to each infinitesimal tape. The way to apply these boundary conditions to each infinitesimal tape is to apply them to the corresponding edges of the bulk, as depicted in figure 7. The resistivity inside the bulk, for the propose of computing T_y , is considered to be the resistivity of the HTS material, thus the strategy proposed here does not consider the copper and other normal conductors that constitute the HTS tapes.

The current density inside the bulk has one component defined by $J_z = \partial T_y / \partial x$. A scaled current density is defined as

$$J_s = \frac{\delta}{\Lambda} J_z \quad (11)$$

where δ is the thickness of a tape and Λ is the thickness of the unit cell. The J_s , for the propose of computing A_z , is impressed in the bulk domain as a source term as follows

$$\nabla^2 A_z = -\mu_0 (\sigma_0 E_z + J_s) \quad (12)$$

where $\sigma_0 = 0$ is the conductivity of the surrounding/non-conductive medium, which for the propose of computing A_z , is considered as the conductivity of the entire bounded universe.

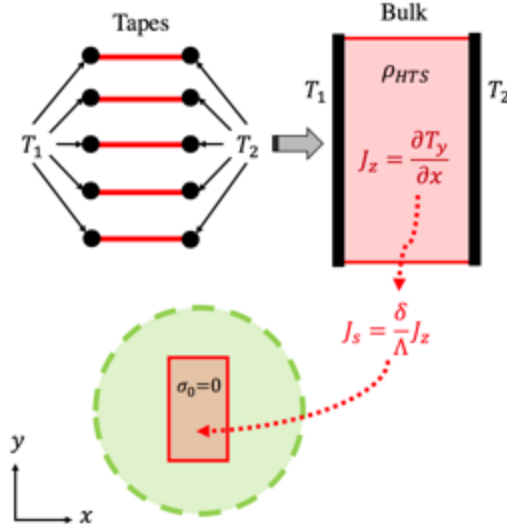


Figure 7. *T-A* homogenization approach. The stack is transformed in a bulk. The influence of the component of B_x is neglected, the T_y is only one component of \mathbf{T} . The boundary conditions T_1 and T_2 should applied to the edges corresponding with the extreme points of the tapes. The scaled current density J_s is impressed as a source term.

Case study *T-A* multi-scale model

The *T-A* multi-scale models in this manuscript consider 30 analyzed tapes, the election of the analyzed tapes follows the same directives proposed in [37], more analyzed tapes are used in the upper part of the pancakes where the results of the full models present higher variations in the losses. The set of analyzed tapes in each pancake is $\{25, 66, 88, 96, 99, 100\}$. This distribution allows reproducing the expected variations in the losses at the upper part of the pancakes.

To avoid the spurious oscillations in J , the unit cells of the analyzed tapes and their closest non-analyzed tapes use second order elements to approximate \mathbf{A} , while first order elements are used to approximate A throughout the rest of the system. The domains using first and second order elements for \mathbf{A} are connected with each other by means of Dirichlet boundary conditions. The analyzed tapes and the domains using second order elements for \mathbf{A} are shown in figure 8. It is important to mention that first order elements are used for \mathbf{T} . The mesh of the unit cells is structured, the mesh of the analyzed tapes and their closest non-analyzed tapes consider 60 elements along the tape's width, while 30 elements are considered along the rest of the tapes. The distribution of the elements along the tape's width is uniform. A part of the mesh presenting these features is also shown in figure 8. The use of first order elements for \mathbf{A} in the non-analyzed tapes as well as less elements along these tapes allows to build a model with less DOF without compromising the accuracy and without spurious oscillations.

Once the hysteresis losses are computed along the analyzed tapes, the Piecewise Cubic Hermite Interpolating Polynomial (PCHIP) method [41] is used to approximate the losses in the non-analyzed tapes.

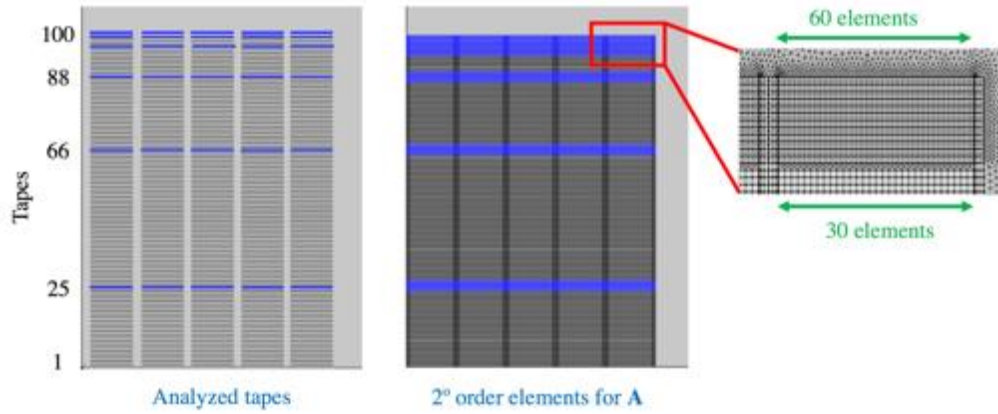


Figure 8. Analyzed tapes, regions with second order elements and the mesh of the T - A multi-scale model. An increased number of analyzed tapes is defined in the upper part of the pancakes. The analyzed tapes and their closet non-analyzed use second order elements for \mathbf{A} . The mesh considers 60 and 30 elements along the tapes.

Case study T - A homogenous model

The T - A homogeneous model of the case study consider 5 bulks, one for each pancake. The mesh in the bulk's domains is structured considering 6 elements along the bulk's width and 60 elements along the tape's width. The distribution of the elements along the bulk's width is similar to the distribution of the analyzed tapes in the multi-scale model, more elements are used in the upper part of the pancakes where the results of the full models present higher variations in the losses. The geometry and the mesh of the model is shown in figure 9. Again, first order elements are used to approximate \mathbf{T} and second order elements for \mathbf{A} .

The hysteresis losses are computed at the center of each of the 6 elements along the bulks. These losses, corresponding to the tapes located at the center of the 6 elements, are used to approximate the losses along the rest of the tapes of the pancakes by means of the PCHIP interpolation method.

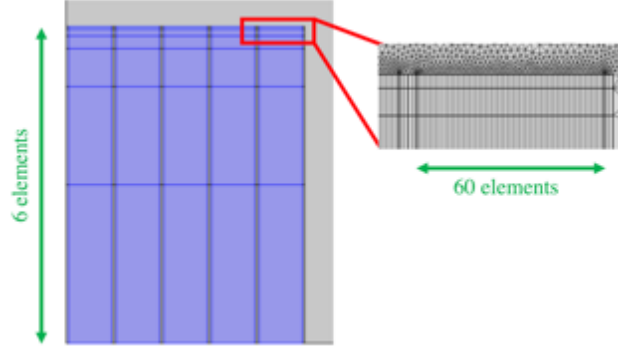


Figure 9. Geometry and mesh of the T - A homogenized model. The bulk's mesh considers 6 elements along the bulks, with a denser distribution of elements in the upper part of the pancakes.

5. Real-time simulations

The real operation of large-scale HTS systems like the scientific magnets involves *slow* charge/discharge cycles, with periods in the order of hours [4]. Assuming such slow transport currents, it is demonstrated here that the T - A multi-scale and T - A homogenous models are so efficient that real-time simulations can be achieved. Real-time simulation means a simulation in which the time required to complete the computation of the output for each time-step is shorter than the actual time-step [42].

T - A full model has been validated against the H full model in section 3. From the analysis presented in the appendix, it is possible to conclude that the computation time required to simulate a *slow* charge/discharge cycle using the H full model becomes prohibitive. Therefore, in this section the T - A full model is used as reference model, to validate the T - A multi-scale and T - A homogeneous models. The T - A models were simulated for the 11 A charge/discharge cycle show in blue line in figure 10, 1 h ramping up, plus 30 min plateau at 11 A, plus 1 h ramping down, plus 30 min plateau. The losses, computed with the three T - A , as a function of time are also shown in the figure 10.

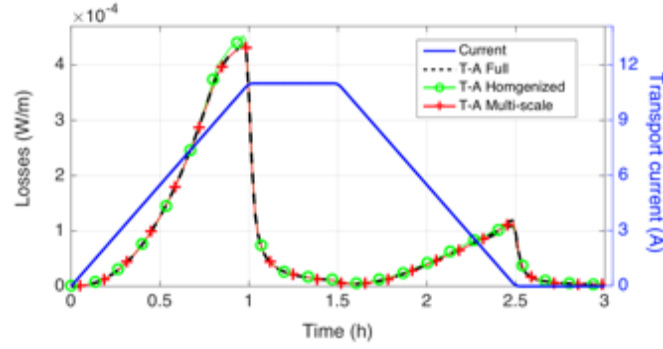
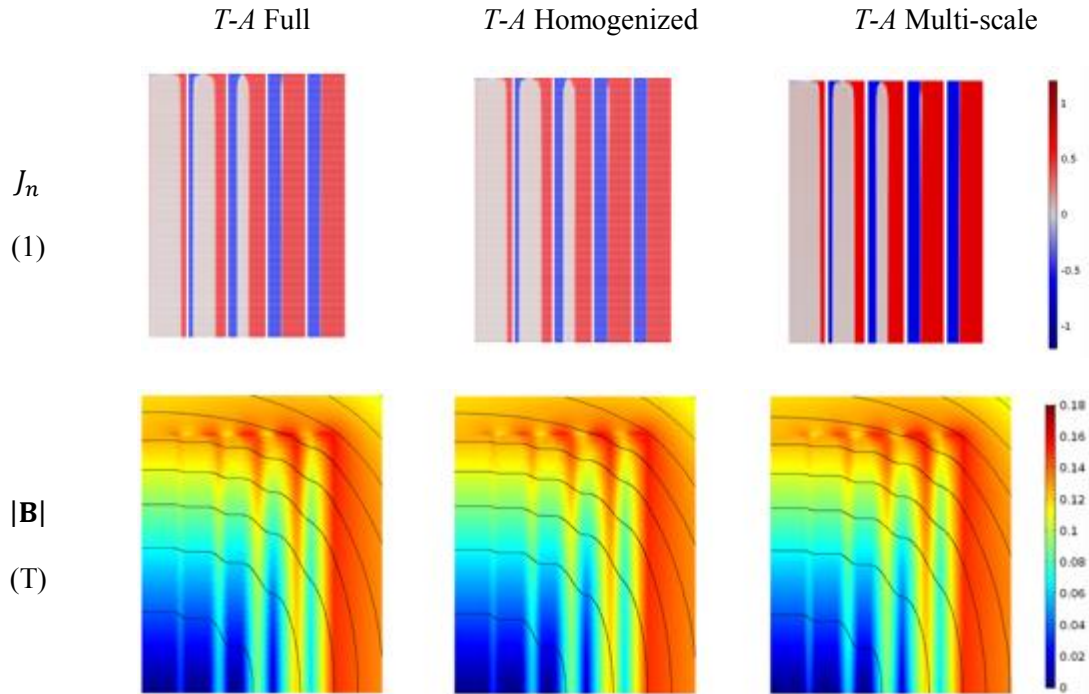


Figure 10. Transport current during the *slow* charging/discharging cycle. Losses as a function of time estimated by the three *T-A* full, multi-scale and homogenous models.

Figure 11 allows making a qualitative comparison between simulation results. The first and second rows present J_n and $|\mathbf{B}|$, respectively, both at the $t = 1.5$ h. It can be seen that the *T-A* multi-scale and homogenous models can successfully reproduce the J distribution produced by the *T-A* full model. The J_n plot of the *T-A* homogeneous model shows the J_n all across the bulks, we decided to present it this way to stress that it corresponds to the *T-A* homogeneous model, but if we had decided to present the plot with the J_n only across the tape domains, the plot would be also indistinguishable from the other two J_n plots. As a direct consequence of the accurate estimation of the J distributions accomplished by the multi-scale and the homogenous models, the magnetic field plots match perfectly at simple sight, this fact constitutes a first validation of both approaches. The third row in figure 11 shows the hysteresis losses integrated all over the charge/discharge cycle. The losses plots show a very good agreement of the losses estimated along each individual tape.



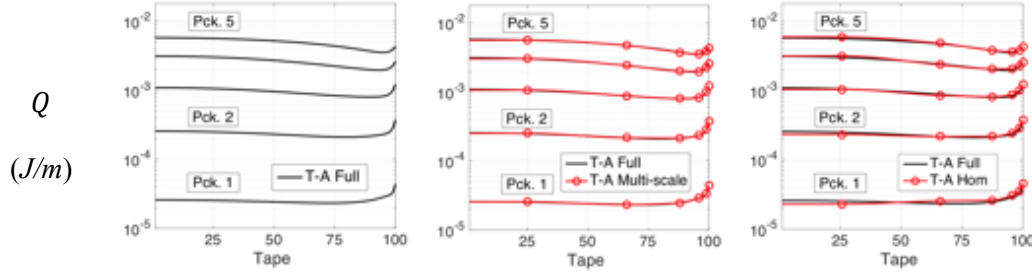


Figure 11. *T-A* full, multi-scale and homogenous models results with a charge/discharge transport current. The first column shows the results of the *T-A* full model. The second, third and fourth row shows the results of *T-A* multi-scale and homogenized models, respectively. The plots for J_n and $|B|$ show the results at peak transport current, $t=1.5$ h. The third row show the losses integrated all over the cycle.

The losses during the 3 h of the analyzed lapse, the losses relative error, the R^2 , and the computation time are summarized in table 3. The estimated losses by both models the *T-A* multi-scale and *T-A* homogeneous agree with the *T-A* full model with 0.28 % and 2.23 %, respectively. Also, both R^2 values are higher than 0.95, these values demonstrate a good agreement in the J estimation. Even though both multi-scale and homogenous models have an acceptable performance, the data in table 3 show that the losses and J distributions of the multi-scale model are more accurate.

The most important result is the achieved computation times, 1h 13 min and 37 min, for the multi-scale and homogeneous models, respectively. Both times are less than the actual simulated time (3 h). Thus, both models are suitable for performing real-time simulations. It is important to mention that the homogeneous model is the less accurate, but at the same time faster. If necessary, the DOF and consequently the computation time can be further reduced for both multi-scale and homogeneous models. The homogeneous model can be reduced by reducing the number of elements along the bulk. The multi-scale model can be reduced, by reducing the number of analyzed tapes, especially in the central pancakes where the losses are lower and do not have a significant impact in the total losses. While it is possible to reduce the DOF in the models, the excessive reduction would compromise the accuracy.

Table 3. *T-A* full, multi-scale and homogenous models comparison.

Model	Losses (J/m)	Relative error (%)	R^2 of J	Computation time
<i>T-A</i> full	0.8832	-	-	9h 04min
<i>T-A</i> multi-scale	0.8807	0.28	0.9888	1h 13min
<i>T-A</i> homogeneous	0.9029	2.23	0.9561	0h 37min

To conclude the discussion of the advantages and disadvantages of the different models, we add a comment about how difficult is to build the models. It is not possible to be categorical, because it strongly depends on the expertise of the analyzer, but some points can be outlined. The models have in common that they require a patient labor to build the geometry and the structured meshes, but this step is particularly easy for the homogeneous model because the number of figures is considerably

lower. The H full model requires the definition of one integral constraint per tape to impress the transport current, this is a time-consuming process. Conversely, the definition of the boundary conditions that fix the transport current in each tape of the T - A full model is a simple process that can be done quickly by means of arrays. Once again, this process is easier in the homogeneous model, because the boundary conditions are defined in the bulks not in the tapes. The T - A multi-scale models require the definition of boundary conditions just at the analyzed tapes, but it is necessary to face the additional complication of defining the functions required to implement the J interpolation.

6. Conclusions

The T - A formulation successfully benefits from the homogenization and multi-scale methods to provide quick and accurate results in large-scale HTS systems. Both the multi-scale and homogeneous models were previously used with the H formulation. In this work we have investigated the required considerations to apply these concepts together with the T - A formulation. These new strategies allow building more efficient models.

The T - A multi-scale method described in this manuscript can be seen as an enhanced version of the iterative multi-scale method [31]. The T - A formulation allows for the simultaneous computation of \mathbf{T} and \mathbf{A} in one single model, thus the T - A multi-scale models do not rely on the iterative implementation of n dynamic simulations of two submodels. Also, the T - A multi-scale models are easier to construct, because there is only one model instead of two submodels.

The analyses conducted in this manuscript show that the assumptions considered in the T - A homogenized and multi-scale models significantly reduce the computation time. These simplifications in the description of the systems do not compromise the accuracy of the results, and not only it is possible to accurately estimate the losses, but also the J distribution. The availability of the T - A homogenized and multi-scale models opens the possibility for the real-time simulation of large-scale superconductor systems. To the best of our knowledge, this capability is new in the analysis of such complex systems.

Appendix

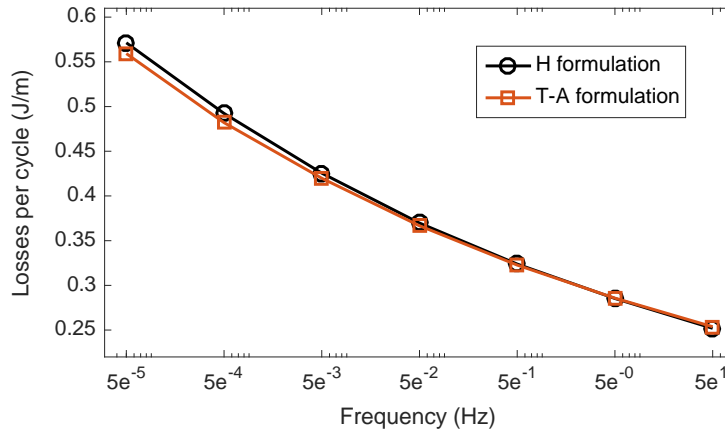
The HTS system models using the H formulation [26] are not proper to conduct simulations of large-scale HTS systems under slow dynamic conditions, because the computation time increases as the frequency decreases. Conversely, the models using the T - A formulation are suitable to simulate such cycles, while keeping the computation time within reason. Here we use the *benchmark #3* of the *HTS modelling workgroup* [43] to study the enlargement of the computation time required to simulate a sinusoidal cycle when the frequency is gradually reduced.

The *benchmark 3#* is a 20 tapes stack representative of a racetrack coil. The parameters of *benchmark 3#* are resumed in table A1. Two models are built, the first model is a H formulation model and the second is a T - A formulation model, both models considering each tape, thus can be called H *full* and T - A *full* models, respectively. The mesh used in both models is structured and considers 60 elements along the tape's width.

Table A1. Benchmark 3# parameters.

Parameter	Value
Tapes	20
Inner radius	10 cm
HTS layer width	12 mm
HTS layer thickness	1 μm
Distance between tapes	250 μm
I_c	300 A
N	25

The conducted simulations consider $0.5 \cdot I_c = 150$ A sinusoidal transport currents, with frequencies ranging from $5 \cdot 10^{-5}$ Hz to 50 Hz. The hysteresis losses per cycle and the computation time as a function of frequency are shown figure A1 and A2, respectively. The results in figure A1 show that the losses per cycle have a small frequency dependence, similar results have been reported in [44-47]. Figure A2 show that the computation time required to simulate one sinusoidal cycle using the *T-A full* model is independent of the frequency, and remains around 300 s for all the frequency range. On the contrary, the computation time required by the *H full* model expands up to 36.6 h when the frequency is $5 \cdot 10^{-5}$ Hz.

**Figure A1.** Benchmark #3. Losses per cycle as a function of frequency.

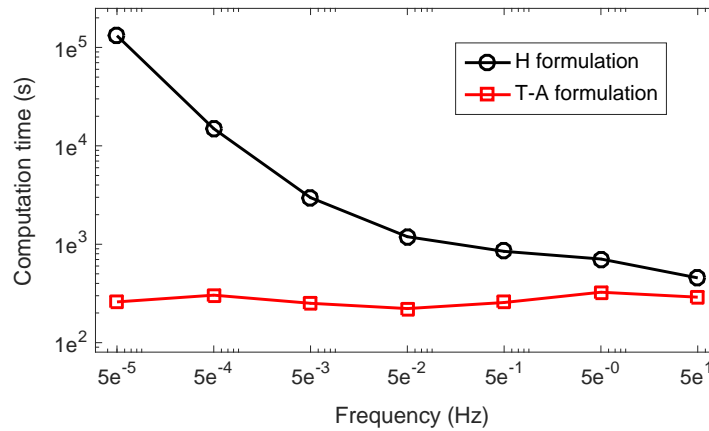


Figure A2. Benchmark #3. Computation time required to simulate one sinusoidal cycle as a function of frequency.

References

- [1] Melhem Z 2012 *High temperature superconductors (HTS) for energy applications* (Cambridge, U.K.: Woodhead Publishing).
- [2] Markiewicz, W., Larbalestier, D., Weijers, H., Voran, A., Pickard, K., Sheppard, W., Jaroszynski, J., Aixia Xu, Walsh, R., Jun Lu, Gavrilin, A. and Noyes, P. (2012). Design of a Superconducting 32 T Magnet With REBCO High Field Coils. *IEEE Transactions on Applied Superconductivity*, 22(3), pp.4300704-4300704.
- [3] Weijers, H., Markiewicz, W., Gavrilin, A., Voran, A., Viouchkov, Y., Gundlach, S., Noyes, P., Abraimov, D., Bai, H., Hannahs, S. and Murphy, T. (2016). Progress in the Development and Construction of a 32-T Superconducting Magnet. *IEEE Transactions on Applied Superconductivity*, 26(4), pp.1-7.
- [4] Xia, J., Bai, H., Lu, J., Gavrilin, A., Zhou, Y. and Weijers, H. (2015). Electromagnetic modeling of REBCO high field coils by the H-formulation. *Superconductor Science and Technology*, 28(12), p.125004.
- [5] Norris, W. (1970). Calculation of hysteresis losses in hard superconductors carrying ac: isolated conductors and edges of thin sheets. *Journal of Physics D: Applied Physics*, 3(4), pp.489-507.
- [6] Halse, M. (1970). AC face field losses in a type II superconductor. *Journal of Physics D: Applied Physics*, 3(5), pp.717-720.
- [7] Brandt, E. (1994). Thin superconductors in a perpendicular magnetic ac field: General formulation and strip geometry. *Physical Review B*, 49(13), pp.9024-9040.

- [8] Mawatari, Y. (1996). Critical state of periodically arranged superconducting-strip lines in perpendicular fields. *Physical Review B*, 54(18), pp.13215-13221.
- [9] Müller, K. (1997). Self-field hysteresis loss in periodically arranged superconducting strips. *Physica C: Superconductivity*, 289(1-2), pp.123-130.
- [10] Müller, K. (1999). AC losses in stacks and arrays of YBCO/hastelloy and monofilamentary Bi-2223/Ag tapes. *Physica C: Superconductivity*, 312(1-2), pp.149-167.
- [11] Clem, J. (2008). Field and current distributions and ac losses in a bifilar stack of superconducting strips. *Physical Review B*, 77(13).
- [12] Mikitik, G., Mawatari, Y., Wan, A. and Sirois, F. (2013). Analytical Methods and Formulas for Modeling High Temperature Superconductors. *IEEE Transactions on Applied Superconductivity*, 23(2), pp.8001920-8001920.
- [13] Bastos, J. and Sadowski, N. (2003). *Electromagnetic modeling by finite element methods*. New York: Marcel Dekker.
- [14] Jin, J. (n.d.). *The Finite Element Method in Electromagnetics*.
- [15] Jin, J. (2015). *Theory and computation of electromagnetic fields*. Hoboken: Wiley.
- [16] Sirois, F. and Grilli, F. (2015). Potential and limits of numerical modelling for supporting the development of HTS devices. *Superconductor Science and Technology*, 28(4), p.043002.
- [17] Grilli, F. (2016). Numerical modeling of HTS applications. *IEEE Transactions on Applied Superconductivity*, pp.1-1.
- [18] Grilli, F., Pardo, E., Stenvall, A., Nguyen, D., Weijia Yuan and Gomory, F. (2014). Computation of Losses in HTS Under the Action of Varying Magnetic Fields and Currents. *IEEE Transactions on Applied Superconductivity*, 24(1), pp.78-110.
- [19] Quéval, L., Zerméño, V. and Grilli, F. (2016). Numerical models for ac loss calculation in large-scale applications of HTS coated conductors. *Superconductor Science and Technology*, 29(2), p.024007.
- [20] Pardo, E., Gömöry, F., Šouc, J. and Ceballos, J. (2007). Current distribution and ac loss for a superconducting rectangular strip with in-phase alternating current and applied field. *Superconductor Science and Technology*, 20(4), pp.351-364.
- [21] Pardo, E. (2013). Calculation of AC loss in coated conductor coils with a large number of turns. *Superconductor Science and Technology*, 26(10), p.105017.
- [22] Pardo, E., Šouc, J. and Frolek, L. (2015). Electromagnetic modelling of superconductors with a smooth current–voltage relation: variational principle and coils from a few turns to large magnets. *Superconductor Science and Technology*, 28(4), p.044003.

- [23] E. Pardo, M. Kapolka, and J. Souc, "3D and 2D electromagnetic modelling of superconductors: Flux cutting effects in finite samples and coated conductor coils up to 10 000 turns," in *Proc. 12th Eur. Conf. Appl. Supercond.*, Lyon, France, Sep. 6–10, 2015.
- [24] Amemiya, N., Murasawa, S., Banno, N. and Miyamoto, K. (1998). Numerical modelings of superconducting wires for AC loss calculations. *Physica C: Superconductivity*, 310(1-4), pp.16-29.
- [25] Nibbio, N., Stavrev, S. and Dutoit, B. (2001). Finite element method simulation of AC loss in HTS tapes with B-dependent E-J power law. *IEEE Transactions on Applied Superconductivity*, 11(1), pp.2631-2634.
- [26] Brambilla, R., Grilli, F. and Martini, L. (2006). Development of an edge-element model for AC loss computation of high-temperature superconductors. *Superconductor Science and Technology*, 20(1), pp.16-24.
- [27] Zhang, H., Zhang, M. and Yuan, W. (2016). An efficient 3D finite element method model based on the T–A formulation for superconducting coated conductors. *Superconductor Science and Technology*, 30(2), p.024005.
- [28] Liang, F., Venuturumilli, S., Zhang, H., Zhang, M., Kvitkovic, J., Pamidi, S., Wang, Y. and Yuan, W. (2017). A finite element model for simulating second generation high temperature superconducting coils/stacks with large number of turns. *Journal of Applied Physics*, 122(4), p.043903.
- [29] Fenicsproject.org. (2018). *Solving PDEs in Python - The FEniCS Tutorial Volume I*. [online] Available at: https://fenicsproject.org/pub/tutorial/html/_ftut1009.html [Accessed 3 Oct. 2018].
- [30] P. Hood and C. Taylor, *Navier-Stokes equations using mixed interpolation*, in *Finite Element Methods in Flow Problems*, J. T. Oden, R. H. Gallagher, O. C. Zienkiewicz, and C. Taylor, eds., University of Alabama in Huntsville Press, 1974, pp. 121-132.
- [31] Clem, J., Claassen, J. and Mawatari, Y. (2007). AC losses in a finiteZstack using an anisotropic homogeneous-medium approximation. *Superconductor Science and Technology*, 20(12), pp.1130-1139.
- [32] Yuan, W., Campbell, A. and Coombs, T. (2009). A model for calculating the AC losses of second-generation high temperature superconductor pancake coils. *Superconductor Science and Technology*, 22(7), p.075028.
- [33] Prigozhin, L. and Sokolovsky, V. (2011). Computing AC losses in stacks of high-temperature superconducting tapes. *Superconductor Science and Technology*, 24(7), p.075012.
- [34] Zermeno, V., Abrahamsen, A., Mijatovic, N., Jensen, B. and Sørensen, M. (2013). Calculation of alternating current losses in stacks and coils made of second generation high temperature superconducting tapes for large scale applications. *Journal of Applied Physics*, 114(17), p.173901.

- [35] Queval, L. and Ohsaki, H. (2013). AC Losses of a Grid-Connected Superconducting Wind Turbine Generator. *IEEE Transactions on Applied Superconductivity*, 23(3), pp.5201905-5201905.
- [36] Quéval, L., Zerméño, V. and Grilli, F. (2016). Numerical models for ac loss calculation in large-scale applications of HTS coated conductors. *Superconductor Science and Technology*, 29(2), p.024007.
- [37] Berrospe-Juarez, E., Zerméño, V., Trillaud, F. and Grilli, F. (2018). Iterative multi-scale method for estimation of hysteresis losses and current density in large-scale HTS systems. *Superconductor Science and Technology*, 31(9), p.095002.
- [38] Rhyner, J. (1993). Magnetic properties and AC-losses of superconductors with power law current-voltage characteristics. *Physica C: Superconductivity*, 212(3-4), pp.292-300.
- [39] Kim, Y., Hempstead, C. and Strnad, A. (1962). Critical Persistent Currents in Hard Superconductors. *Physical Review Letters*, 9(7), pp.306-309.
- [40] Chapra, S. and Canale, R. (2010). *Numerical methods for engineers*. Boston, Mass.: McGraw-Hill Higher Education.
- [41] De.mathworks.com. (2018). Piecewise Cubic Hermite Interpolating Polynomial (PCHIP) - MATLAB pchip- MathWorks Deutschland. [online] Available at: <https://de.mathworks.com/help/matlab/ref/pchip.html> [Accessed 28 Jul. 2018].
- [42] Omar Faruque, M., Strasser, T., Lauss, G., Jalili-Marandi, V., Forsyth, P., Dufour, C., Dinavahi, V., Monti, A., Kotsampopoulos, P., Martinez, J., Strunz, K., Saeedifard, M., Xiaoyu Wang, Shearer, D. and Paolone, M. (2015). Real-Time Simulation Technologies for Power Systems Design, Testing, and Analysis. *IEEE Power and Energy Technology Systems Journal*, 2(2), pp.63-73.
- [43] Htsmodelling.com. (2018). *HTS MODELING WORKGROUP: Benchmarks*. [online] Available at: http://www.htsmodelling.com/?page_id=2 [Accessed 22 Nov. 2018].
- [44] Sander, M. and Grilli, F. (2010). FEM-calculations on the frequency dependence of hysteretic losses in coated conductors. *Journal of Physics: Conference Series*, 234(2), p.022030.
- [45] Thakur, K., Raj, A., Brandt, E., Kvitkovic, J. and Pamidi, S. (2011). Frequency-dependent critical current and transport ac loss of superconductor strip and Roebel cable. *Superconductor Science and Technology*, 24(6), p.065024.
- [46] Thakur, K., Raj, A., Brandt, E. and Sastry, P. (2011). Frequency dependent magnetization of superconductor strip. *Superconductor Science and Technology*, 24(9), p.099501.
- [47] Sirois, F., Grilli, F. and Morandi, A. (2018). Comparison of Constitutive Laws for Modeling High-Temperature Superconductors. *IEEE Transactions on Applied Superconductivity*, 29(1), pp.1-10.